Exploring Non-Stoichiometric Nickel Oxide (NiO_x) as a Hole Transport Layer for Cesium Tin Triiodide ($CsSnI_3$) Perovskite Solar Cells

Jacob Albrikan

A thesis

submitted in partial fulfillment of

the requirements for the degree of

Master of Science in Chemical Engineering

University of Washington

2020

Committee:

Professor Qiuming Yu (Chair)

Professor René Overney

Program Authorized to Offer Degree:

Chemical Engineering

University of Washington

Abstract

Exploring Non-Stoichiometric Nickel Oxide (NiO_x) as a Hole Transport Layer for Cesium Tin Triiodide ($CsSnI_3$) Perovskite Solar Cells

Jacob Albrikan

Chair of the Supervisory Committee:

Professor Qiuming Yu

Department of Chemical Engineering

Inverted planar $CsSnI_3$ perovskite p-i-n structure shows a high potential as a candidate for inorganic lead-free perovskite solar cells (PVSCs). Nickel oxide (NiO_x) offers promising characteristics for a winning hole transport layer (HTL), such as high optical transmittance, high stability, easy processability, and a wide band gap that allows high hole mobility and good electron blocking ability. In this work, NiO_x was synthesized by first forming $Ni(OH)_2$ in the precipitation reaction of ($Ni(NO_3)_2 \cdot 6H_2O$) and NaOH. The synthesized NiO_x nanocrystals was dissolved in DI water to different concentrations and used as a HTL in the inverted p-i-n $CsSnI_3$ PVSCs. The effects of annealing condition, concentration of NiO_x ink and spin speed on the NiO_x film morphology and surface roughness were explored. In addition, $CsSnI_3$ thin films were fabricated to be the active layer and solar cells with the inverted structure were fabricated and tested.

LIST OF FIGURES

ACKNOWLEDGEMENT

I would like to express my deepest appreciation to my advisor Professor Qiuming Yu for her help, guidance, and encouragement, my group members, Gabriella Tosado, Erjin Zheng, Zhiyin Niu, Emerson Chen, Zonglun Li, Zizhao Xu, and Shukun Zhong, for their support and ideas, and my parents for their unconditional support and encouragement. Also, I would like to thank Professor René Overney for being a committee member.

Chapter 1. Introduction

Perovskite solar cells have been widely explored in the past eight years, and there has been a significant progress in the realm. Inorganic-organic halide perovskites have several advantages, such as strong optical absorption, very small exciton binding energy, high carrier mobility, long lifetime and diffusion length, which make them promising for the photovoltaic applications. The power conversion efficiency (PCE) of perovskite solar cells has increased from 2.2% to 23% and still has the potential to increase more.[1] The most common type of the perovskite active layer is the organometallic hybrid perovskites, which contain methylammonium (MA^+) and formamidinium (FA^+), or a mix of the two cations, lead as a metal and halides such as I^- and Br^-. Despite the impressive progress in lead-based perovskite solar cells, a significant drawback is the toxicity of dissolvable lead content in these materials. When soil and water become polluted with lead and its compounds, it can result in a long-term environmental damage and a serious harm to humans. When lead enters the human body, it targets the nervous and productive system causing a severe damage over time as lead stays in the human body for very long time. Due to the concern of lead toxicity, the use of the lead-based perovskite solar cells in large-scale industrial applications is hindered.[2] Therefore, finding lead alternatives has been the interest of many researchers in the recent years. One of these cleaner alternatives is tin as it has a similar electronic structure to lead and tin based perovskites have a narrower band gap, low exciton binding energies, and longer carrier diffusion length than their equivalent lead-based perovskite.[3-5] In particular, all inorganic tin-based perovskite $CsSnI_3$ has been selected as the active layer in this work because it has a band gap (E_g) of 1.3 eV, which is close to the optimal for perovskite photovoltaics.[11]

poly(3,4-ethylenedioxythiophene) polystyrene sulfonate (PEDOT:PSS) has been the most commonly used hole transport layer (HTL) for inverted planar structured perovskite solar cells. PEDOT:PSS has several advantages that make it a suitable HTL, such as high work function, high transparency, and high conductivity. However, PEDOT:PSS has an acidic and hygroscopic characteristics that decrease the device stability and cause the device to degrade. When PEDOT:PSS is added on ITO coated glass surface, the interface between ITO and PEDOT:PSS is not stable due to the acidic PEDOT:PSS etching of the ITO. Therefore, there has been a significant interest to find a more stable alternative to PEDOT:PSS, which has a similar potential to be used as an HTL. Metal oxides have been recognized as a suitable electron/hole transport layer (ETL/HTL) or an electron/hole extraction layer (EEL/HEL). Metal oxides with one metallic element, such as zinc oxide, tin oxide, titanium oxide, and nickel oxide have been used as interface material because their chemical compositions in film deposition is easier to be controlled than multicomponent oxides.[6] Nickel oxide (NiO_x) offers promising characteristics for a winning HTL, such as high optical transmittance, high stability, easy processability, and a wide band gap that allows high hole mobility and good electron blocking ability.[7-8]

In this project, the intent is to utilize all inorganic materials to make up the hole transport layer and active layer. The active layer used in this project is $CsSnI_3$, the HTL is NiOx, and the ETL is [6,6]-phenyl-C_{60}-butyric acid methyl ester ($PC_{60}BM$). In particular, we synthesized NiO_x nanocrystals (NCs), explored the effect of annealing conditions, concentration of NiO_x ink and spin speed on the NiO_x film morphology and surface roughness. Also, we synthesized $CsSnI_3$ to be the active layer and explored the interaction between the two layers through the device performance.

Chapter 2. Experimental Methods

2.1 Materials

Tin(II) iodide (SnI_2, 99.99%), cesium iodide (CsI, 99.999%), chlorobenzene (CB, ≥99.8%), chloroform (≥99.9%), Dimethylformamide (DMF, ≥99.9%), and Nickel(II) nitrate hexahydrate ($Ni(NO_3)_2 \cdot 6H_2O$, ≥ 99.999%), bathocuproine (BCP, ≥99%), were purchased from Sigma-Aldrich (St. Louis, Missouri), [6,6]-phenyl-C_{60}-butyric acid methyl ester ($PC_{60}BM$ >99.5%) was purchased from American Dye Source (Quebec, Canada), and 2-propanol (IPA, 99.9%) was purchased from Fisher Scientific (Hampton, New Hampshire).

2.2 NiOx nanocrystals (NCs) synthesis

The NiO_x NCs were synthesized by dissolving 5 g of $Ni(NO_3)_2 \cdot 6H_2O$ in 3.1 mL of deionized water to make a 5 M dark green solution. The solution pH was adjusted to 10 by adding 10 M NaOH. The solution color changed to light green indicating the formation of $Ni(OH)_2$ colloidal precipitation. The sol was centrifuged at 10000 rpm for 10 min and the precipitate was collected. Subsequently, the green color supernatant was centrifuged again at 10000 rpm for 10 min and the precipitate was collected. This process was repeated until the supernatant turned to very faded green. The obtained green powder was dried in the vacuum oven at 80^{o}C and atmosphere pressure overnight, followed by baking at 270^o C for 2 h to obtain the dark NiO_x NCs.

2.3 NiOx NC thin film fabrication

NiOx NCs were dispersed in DI water to make different concentrations. For example, 20 mg of NiO_x NCs were dispersed in 1 mL of DI water to make a concentration of 2 wt% NiO_x black ink. The black ink was stirred vigorously at 1000 rpm using a stirrer and stirred overnight. Glass substrates were cut into 1.5 cm × 1.5 cm to be used as a substrate for film characterization. The

substrates were cleaned using ultrasonic cleaner for 15 min in soapy water, DI water, acetone, and iso-propanol in order. Subsequently, the substrates were treated with 100 W oxygen plasma for 10 min. NiO_x ink was ultrasonicated for 3 h and filtered with 0.45 µL PTFE syringe filter. A 70 µL drop of filtered 2 wt% NiO_x ink was added on the glass substrates and spin coated at 1000, 1500, and 2000 rpm for 30 s. Finally, the coated substrates were annealed at 100^oC for 10 min. This process was repeated using 3, 4, 6, and 8 wt% NiO_x ink for making NiO_x films.

2.4 $CsSnI_3$ perovskite thin film fabrication

The perovskite precursor for making $CsSnI_3$ films was prepared in the glovebox by dissolving 0.205 g of SnI_2 in 0.5 mL DMF to make 1 M solution. 10 mol% excess of SnI_2 was used as a reducing agent to prevent the oxidation of Sn^{2+} to Sn^{4+}. The SnI_2 solution was stirred at room temperature for 1 h. The stirred solution was added to 0.130 g of CsI and stirred overnight in the glovebox at room temperature to make a 1 M precursor solution. Glass was cut and cleaned as previously mentioned to be used as a substrate for film characterization. The $CsSnI_3$ precursor was filtered using 0.45 µL PTFE syringe filter and 70 µL of the filtered $CsSnI_3$ precursor was added on glass substrates and spin coated at 500 rpm for 5 s, 1000 rpm for 15 s, and 4000 rpm for 40 s in a nitrogen glovebox. 500 µL of chlorobenzene was used as an antisolvent during the last 15 s of spin coating. Finally, the coated substrates were annealed at 90^oC for 10 min.

2.5 NiOx and $CsSnI_3$ film characterization

Ultraviolet-visible (UV-Vis) absorption spectra were collected using a Varian Cary 5000 UV-Vis-NIR spectrophotometer to determine the band gap of NiO_x and $CsSnI_3$ thin films. Tapping mode atomic force microscopy (TM-AFM) was used to obtain topography and phase images to analyze the morphology and the roughness of the NiO_x films. Scanning electron microscopy (SEM) images

were acquired using a FEI Sirion SEM operated at 5 kV to determine the surface morphology of the NiO_x and $CsSnI_3$ films. Two-dimensional X-ray diffraction (XRD) patterns were collected with a Bruker GADDS D8 Focus Powder Discover diffractometer using Cu Kα radiation (λ = 1.5419 Å) and the data were processed using the EVA package provided by Bruker Axs to investigate the crystalline structures of the $CsSnI_3$ and NiO_x films.

2.6 Device fabrication

ITO coated glass substrates (10 ohm sq^{-1} ITO, Colorado Concept Coatings LLC) were cut and cleaned as previously described. The NiO_x films were fabricated as described in 2.3. The substrates were transferred to the glovebox and the $CsSnI_3$ perovskite thin film was fabricated on top of a NiO_x film as previously described. $PC_{60}BM$ solution (20 mg/ml in chloroform) was filtered using a 0.45 µL PTFE syringe filter. A 65 µL drop of the filtered $PC_{60}BM$ solution was added on the perovskite layer, spin coated at 4000 rpm for 60 s, and dried without annealing. Subsequently, BCP solution (0.5 mg/ml in IPA) was filtered using a 0.45 µL PTFE syringe filter. A 70 µL drop of filtered BCP was added on top of the $PC_{60}BM$ layer, spin coated at 4000 rpm for 60 s, and dried without annealing. Finally, a mask with area holes of 3.14×10^{-6} m^2 was placed on the substrates and 150 nm thick layer of silver that was used as an electrode was deposited by thermal evaporation under high vacuum. The final device structure was Glass/ITO/NiO_x/$CsSnI_3$/$PC_{60}BM$/BCP/Ag.

2.7 Device characterization

The photocurrent density–voltage (J–V) curve measurements were conducted in a N_2 glovebox with a Keithley 2400 Source Meter and a Solar Light Co. Xenon lamp (16S-300 W) and an AM 1.5

filter. Before measurements, the light intensity was calibrated to 100 mW per cm^2 using a standardized National Renewable Energy Laboratory calibrated silicon solar cell.

Chapter 3. Results and Discussion

3.1 NiO_x NCs Characterization

The NiO_x NCs used in this work is the HTL between the perovskite active layer and the ITO electrode. NiO_x was synthesized by first forming $Ni(OH)_2$ in the precipitation reaction of ($Ni(NO_3)_2 \cdot 6H_2O$) and NaOH as shown in Figure 1, steps 1-5. The formed $Ni(OH)_2$ was centrifuged at 10000 rpm for 10 min. The precipitants were collected and steps 4-7 were repeated on the supernatant until the supernatant turned faded green. Subsequently, the obtained $Ni(OH)_2$ was dehydrated at 80°C for 24 h and finally decomposed into the non-stoichiometric nickel oxide (NiO_x) by baking at 270°C for 2 h.

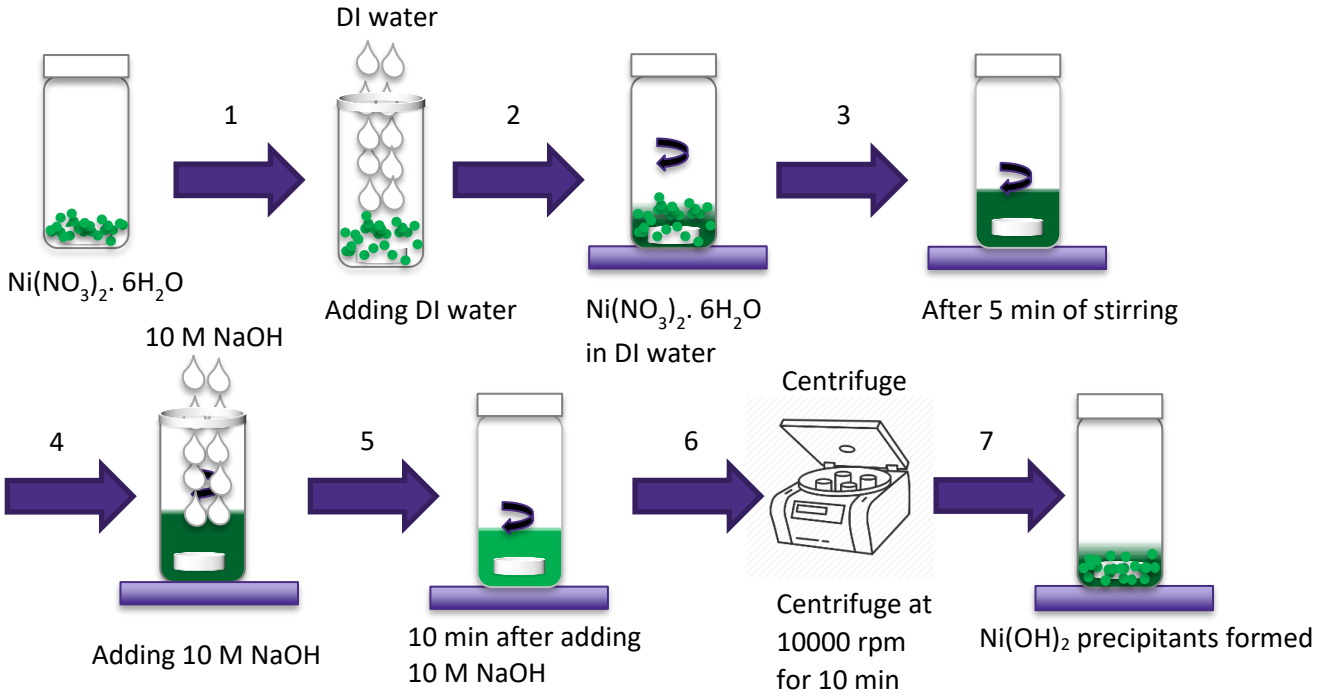

Figure 1. Preparation flowchart of producing $Ni(OH)_2$ that is used to obtain NiO_x.

Figure 2a shows the X-ray diffraction (XRD) pattern of the reference NiOx nanocrystals displaying the reflections of cubic NiO_x at 37.2°, 43.3°, 62.7°, 75.4° and 79.4°, corresponding to the lattice planes of (111), (200), (220), (311), and (222), respectively.[8] Theses peaks also indicate that $Ni(OH)_2$ and $NaNO_3$ impurities are not present in the crystal lattice.[2] Figure 2b shows the XRD pattern of the synthsized NiO_x powder, which matches the XRD patteren found in literature.[2]

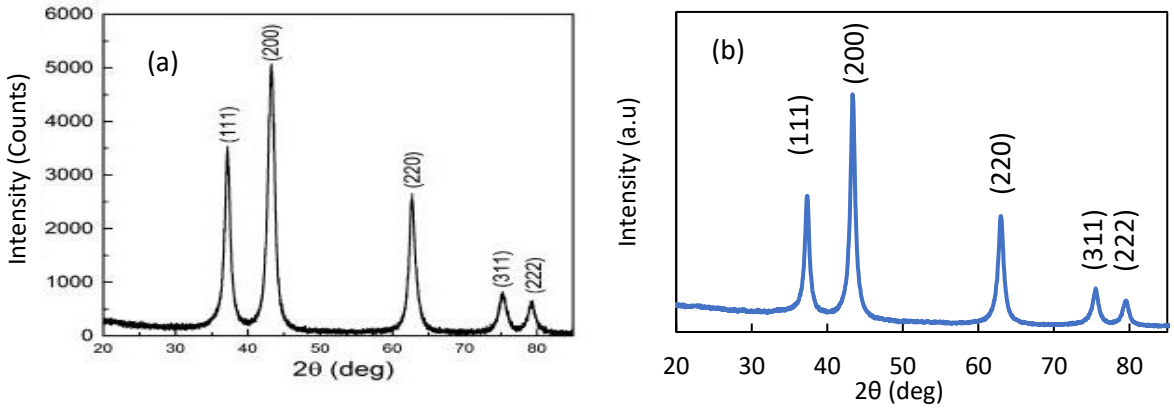

Figure 2. (a) X-ray diffraction (XRD) pattern of the reference NiO_x nanocrystals.[8] (b) XRD pattern of the synthesized NiO_x powder synthesized in this work, which matches the reference XRD pattern.

The UV-Vis absorption spectra of the synthesized NiO_x NCs were acquired to obtain the band gap of the synthesized NiO_x. The synthesized NiO_x NCs were dissolved in DI water to make a total concentration of 2 wt% of the NiO_x ink. The NiO_x ink was diluted to 0.04 wt% by adding 2.4 mL of DI water to 0.1 mL of 2 wt% NiO_x ink. The UV-Vis spectrum in Figure 3 shows a cut-off at 345 nm, which corresponds to 3.59 eV. This value is within 0.1 eV from the band gap value found in literature.[4]

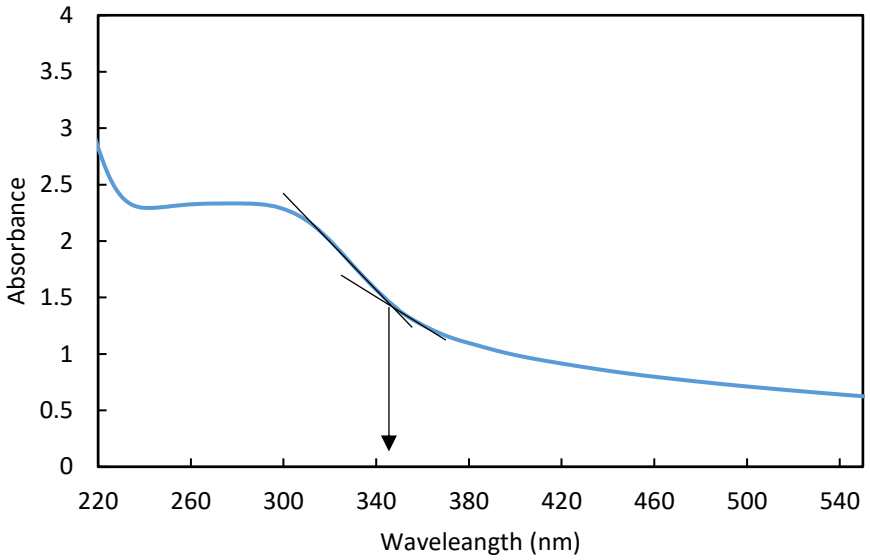

Figure 3. UV-Vis absorption spectrum of 0.04 wt% NiO_x ink in DI water.

3.2 NiO_x thin film fabrication and characterization

NiO_x thin films were formed by spin coating the NiO_x ink onto a cleaned substrate and annealed at 100°C for 10 min. In this work, 2, 3, 4, 6, and 8 wt% of NiO_x ink were explored. The quality of the NiO_x films could be controlled by tuning the concentration of the NiO_x ink and the spin speed. The morphology of the NiO_x films was investigated using AFM and SEM. As shown in the SEM images in Figures 4-6, as the NiO_x concentration increases from 3 to 6 wt%, the film becomes more densely packed and the number of pinholes decreases. The ITO flakes can be seen in the SEM images of Figures 4 and 5. The NiOx films were also prepared using cold drying method by leaving the spin coated film in air for 24 h without annealing. SEM images were obtained to determine if annealing has a significant impact on the NiO_x film morphology. The SEM images of annealed 6 wt% (Figures 6) and unannealed 6 wt% (Figure 7) show that the annealed NiO_x film exhibits more surface coverage and smaller, more uniform particles. Figure 8 shows the AFM topographic images of NiOx films prepared by spin coating the concentration

of NiOx of 2, 4 and 8 wt% on glass substrates. Acquiring the images of the films from 4 and 8 wt% NiOx inks were not stable due to more rough surfaces. From Figure 8, it can be concluded that the concentration of NiO_x influences the film roughness as the concentration of NiO_x increases from 2 to 8 wt%, the film becomes less smooth. The NiOx films were also prepared by using 2 wt% ink but different spin speeds at 1000, 1500, and 2000 rpm. AFM images in Figure 9 shows that the roughness of the film has an insignificant dependence on the spin coating speed of NiO_x.

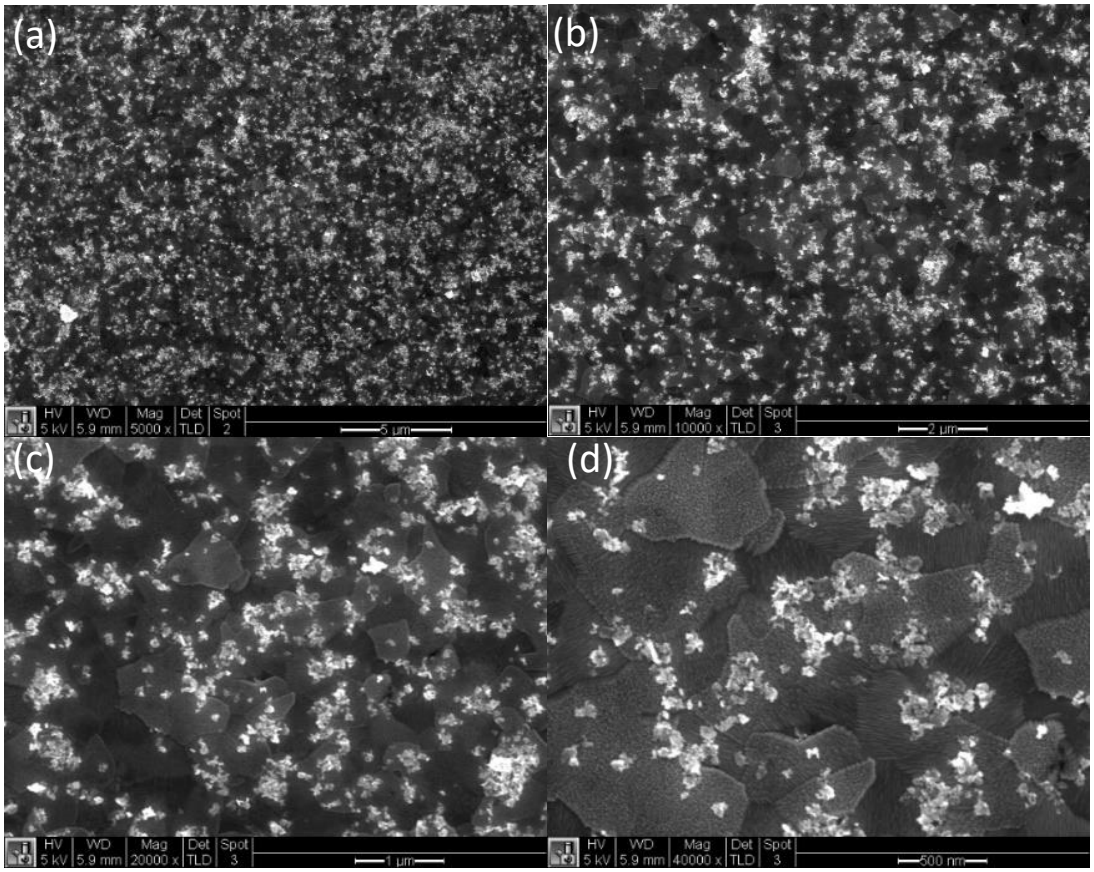

Figure 4. Top view SEM images of annealed 3 wt% NiO_x film with the magnification of (a) 5k, (b) 10k, (c) 20k, and (d) 40k.

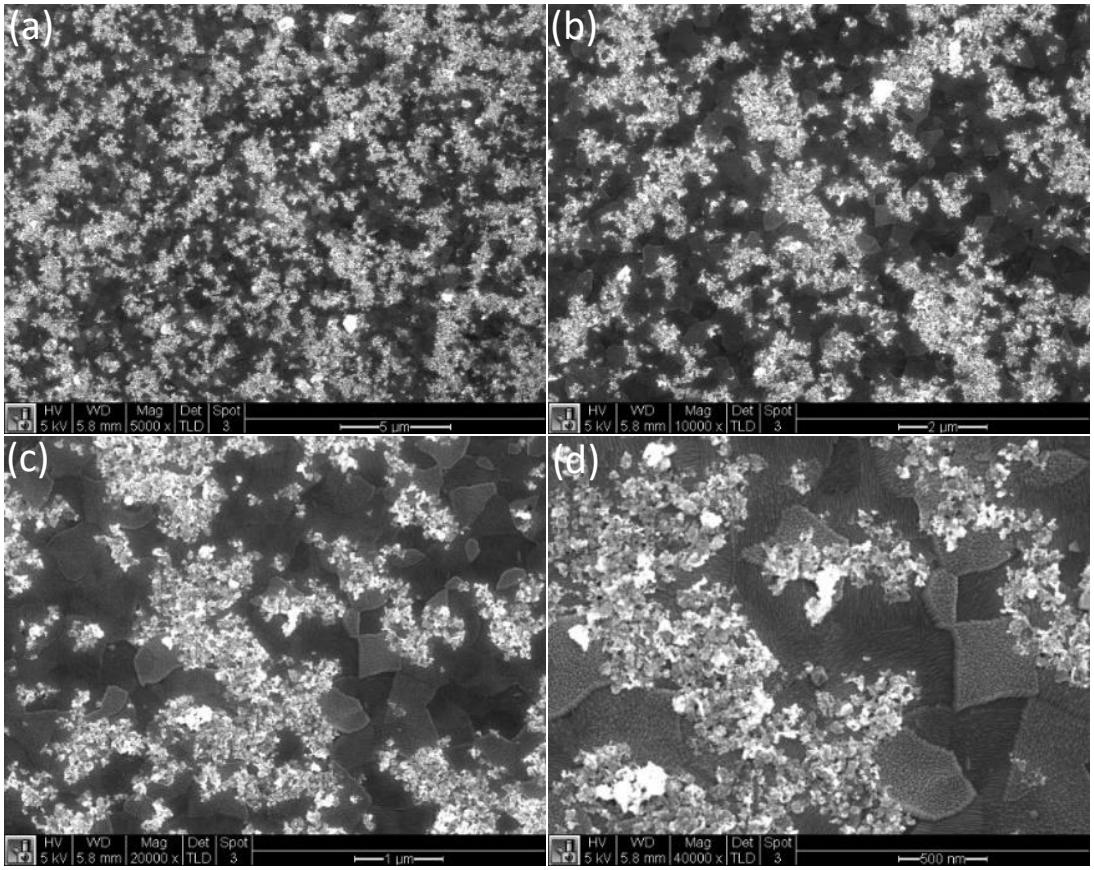

Figure 5. Top view SEM images of annealed 4 wt% NiO_x film with the magnification of (a) 5k, (b) 10k, (c) 20k, and (d) 40k.

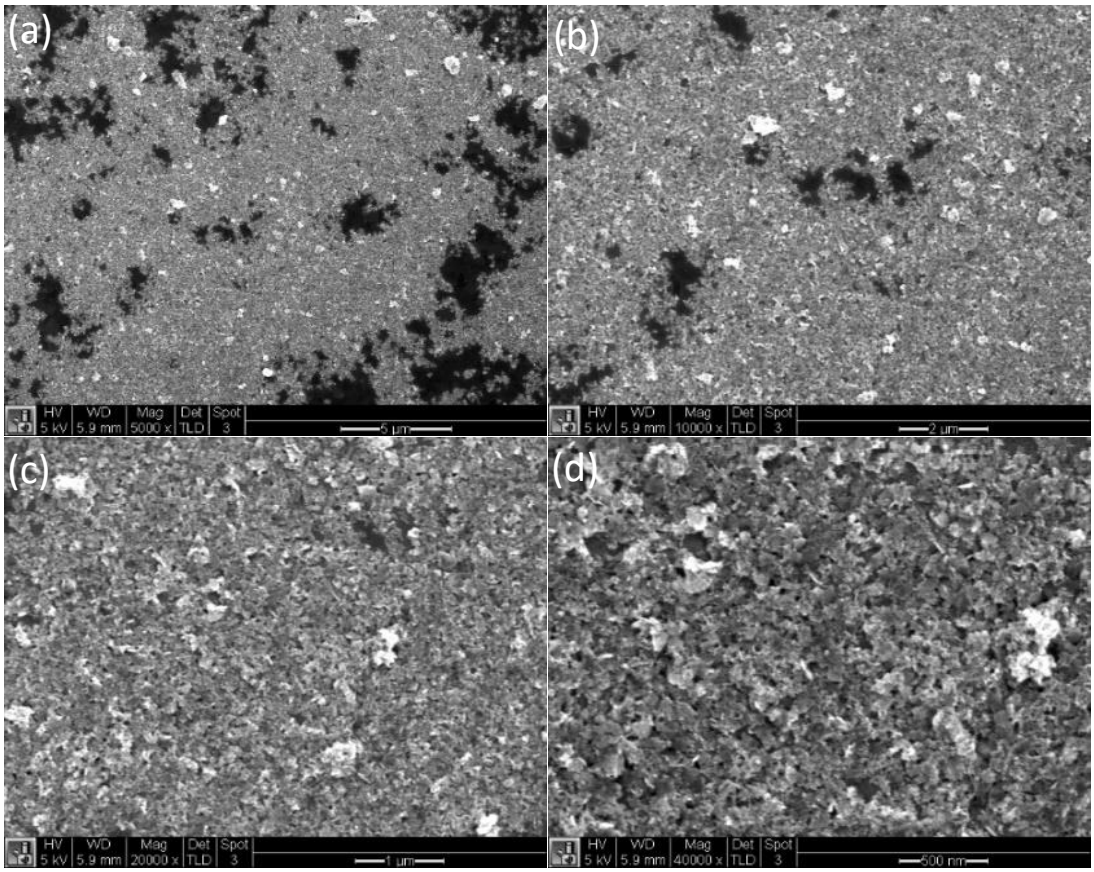

Figure 6. Top view SEM images of annealed 6 wt% NiO_x film with the magnification of (a) 5k, (b) 10k, (c) 20k, and (d) 40k.

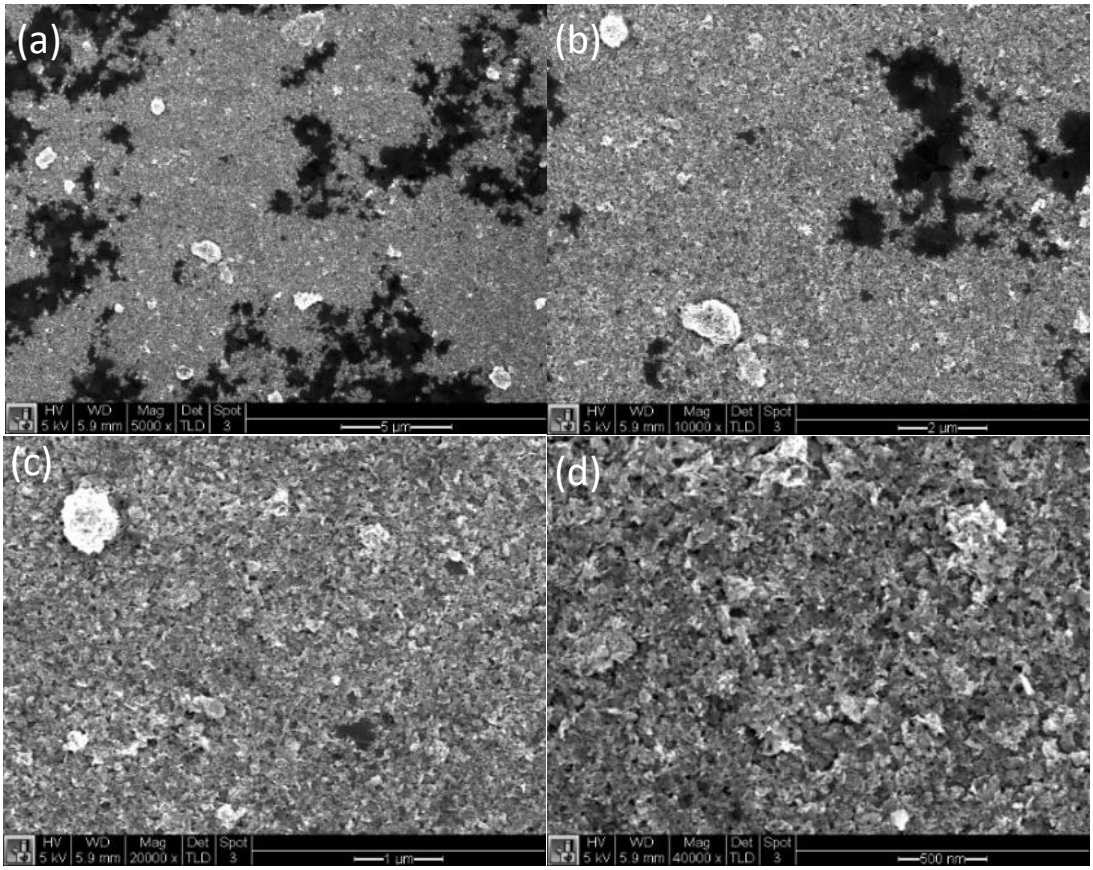

Figure 7. Top view SEM images of unannealed 6 wt% NiO_x film with the magnification of (a) 5k, (b) 10k, (c) 20k, and (d) 40k.

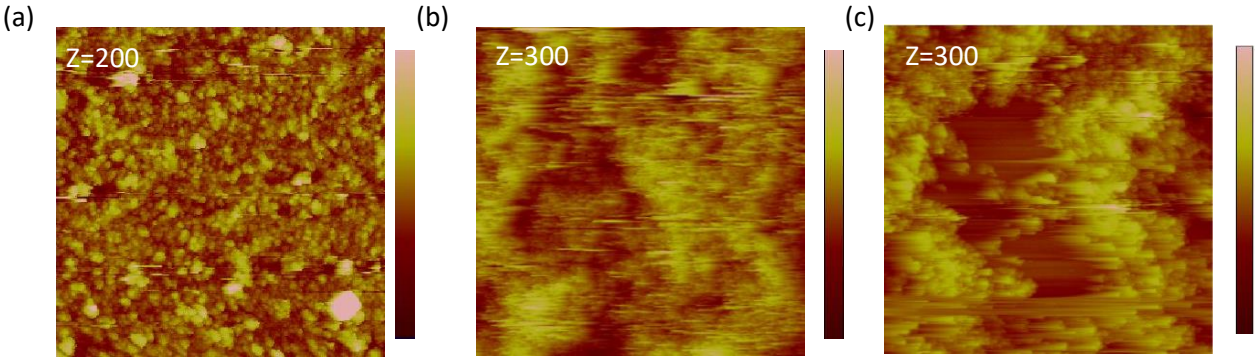

Figure 8. AFM topography images of (a) 2 wt%, (b) 4 wt%, and (c) 8 wt% NiO_x film. The arithmetic average roughness (Ra) values are 13.9, 32, and 35.8 nm, respectively. The image size is 5 µm **x** 5 µm**.** The z scale is 200, 300, and 300, respectively.

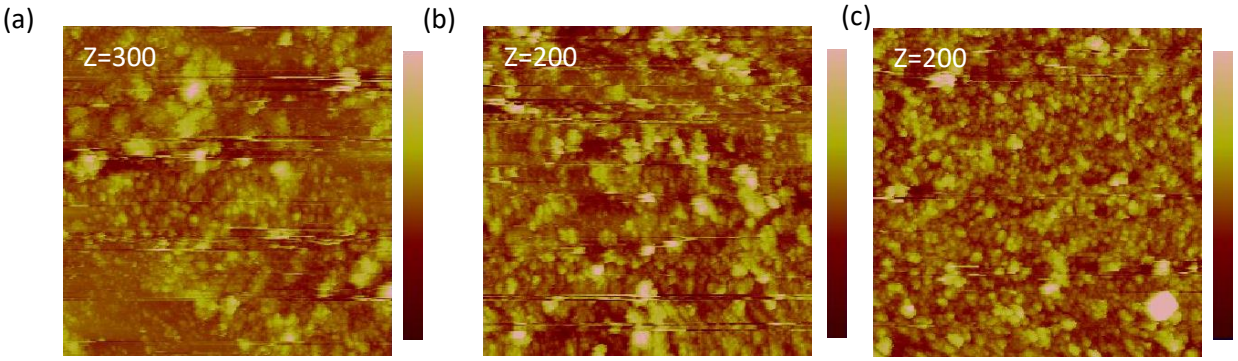

Figure 9. AFM topography images of 2 wt% NiO_x spin coated on glass substrates at spin speed of (a) 1000 rpm, (b) 1500 rpm, and (c) 2000 rpm. The Ra values are 13.9, 13.4, and 14.1 nm, respectively. The image size is 5 µm **x** 5 µm**.** The z scale is 300, 200, and 200, respectively.

The UV-Vis absorption spectra of the NiO_x films were acquired to ensure the accuracy of the band gap of the synthesized NiO_x. NiO_x films with concentrations of 2, 4, and 8 wt% were used as these concentrations were desired to be used for preparing the HTL in the solar cells. The UV-Vis spectra in Figure 10 shows an absorption cut-off at 345 nm, which corresponds to 3.59 eV. This value agrees within 0.1 eV with the band gap value found in literature[4] and matches the bad gap obtained from the solution UV-Vis absorption spectrum shown in Figure 3.

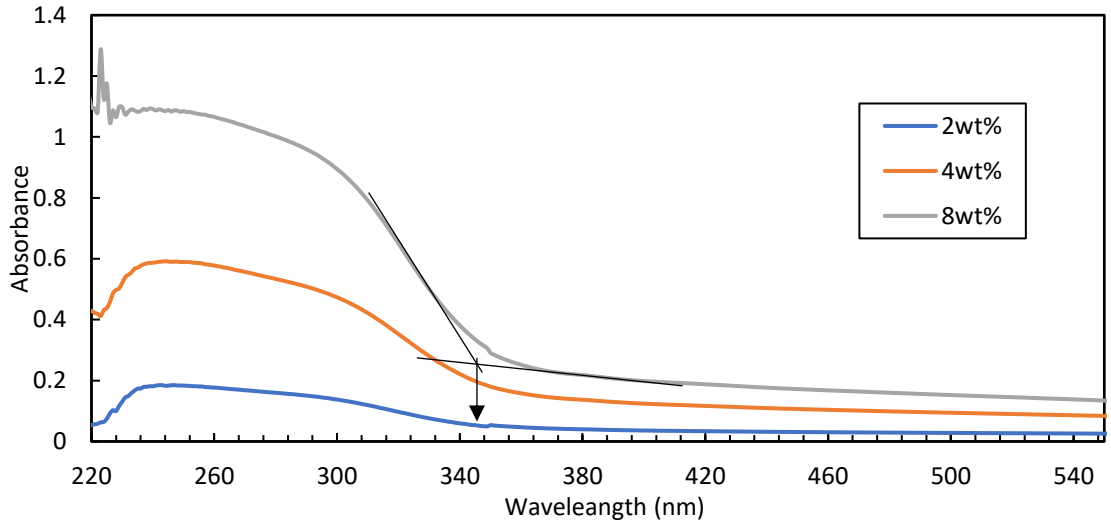

Figure 10. UV-Vis absorption spectra of NiO_x thin films fabricated with 2, 4 and 8 wt% of NiO_x in DI water.

3.3 $CsSnI_3$ thin film fabrication and characterization

$CsSnI_3$ used in this work utilized a one-step solution process with an anti-solvent method to make a dense perovskite thin film. SnI_2 precursor was dissolved in DMF and added to CsI to make a 1 M total concentration with 10 % mole excess of SnI_2. The 10 % mole excess of SnI_2 was used to prevent Sn^{2+} undergo an oxidation reaction to form the more thermodynamically favorable, Sn^{4+}. The films were treated with chlorobenzene in the anti-wash process and annealed at 90^{o}C for 10 min to remove excess DMF and chlorobenzene.

SEM was used to characterize the film morphology and verify the film quality before using it to fabricate the device. As shown in Figure 11a of a large area SEM image, the morphology of the CsSnI3 thin film is densely packed with no apparent pinholes. However, when zooming into the sample further, some pinholes can be seen as displayed in Figures 11b-e. Pinholes could be generated as a result of heterogenous nucleation and different growth rates. Fast growth rate and slow nucleation result in less dense perovskite morphology with larger particles. UV-Vis absorption spectra of $CsSnI_3$ perovskite thin films were obtained to ensure that the band gap of the fabricated film matched literature. From Figure 12, the perovskite shows an absorption cut-off at 982 nm, corresponding to a band gap of 1.3 eV, which agrees with the result found in literature.[11]

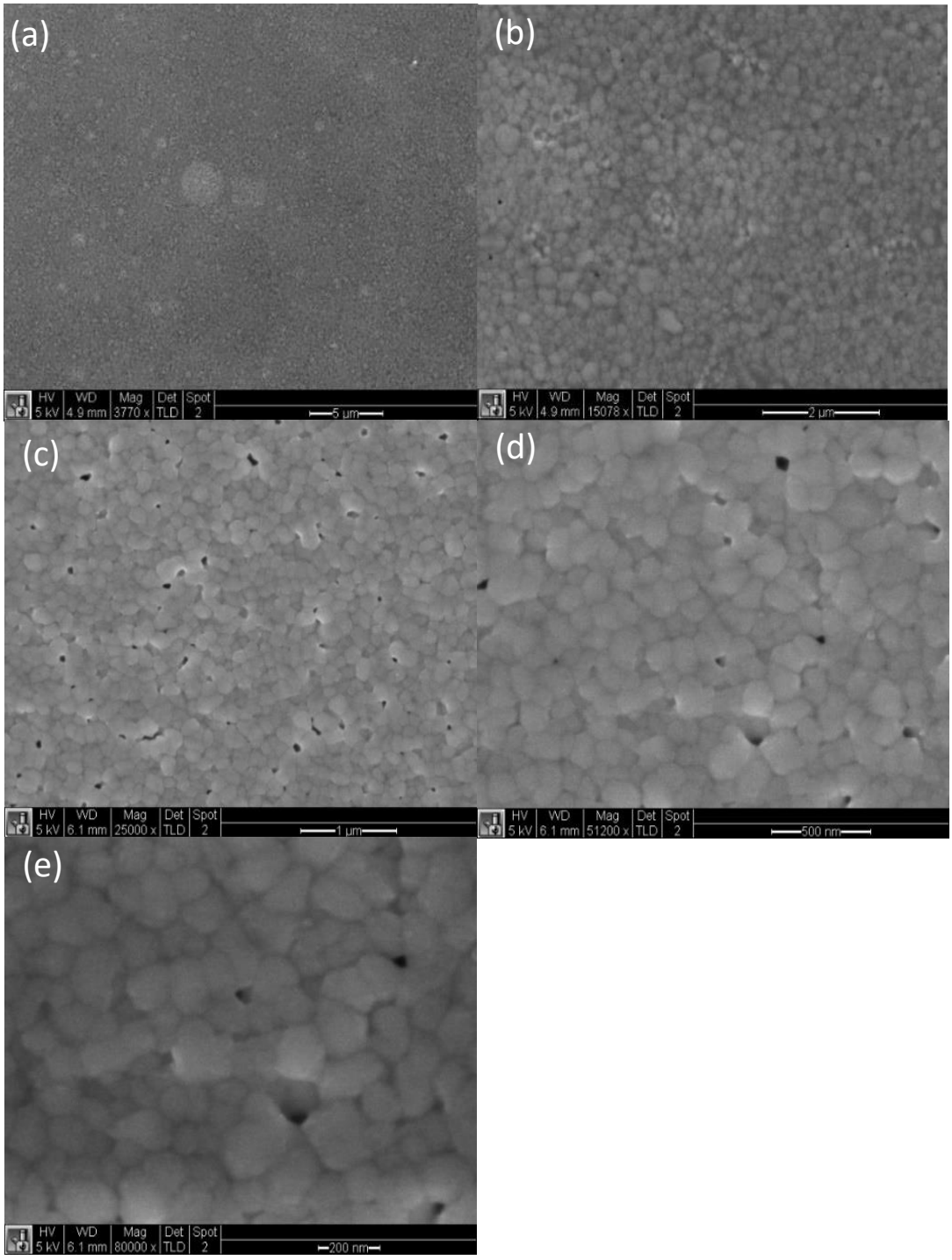

Figure 11. Top view SEM images of $CsSnI_3$ film acquired at different magnifications with the scale bar of (a) 5µm, (b) 2 µm, (c) 1µm, (d) 0.5 µm, and (e) 0.2 µm.

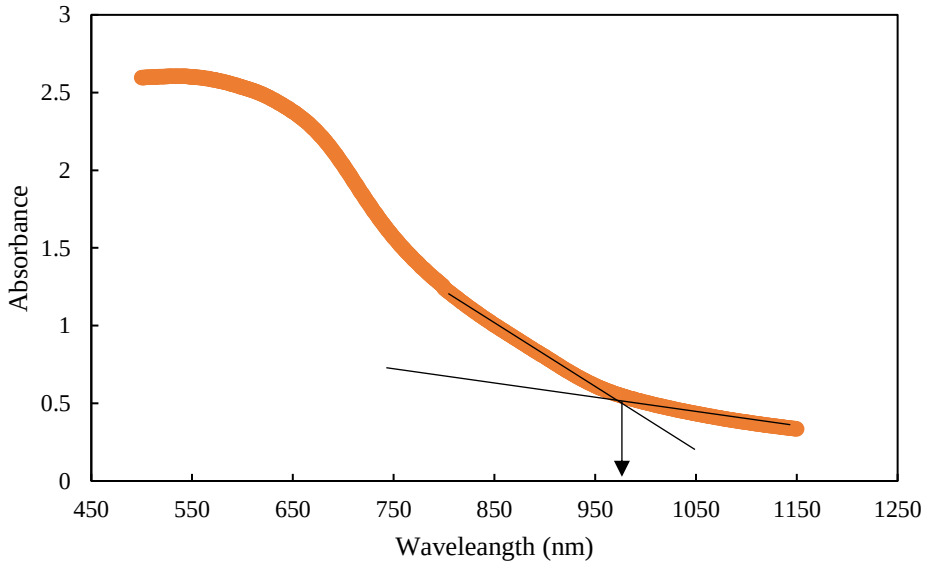

Figure 12. UV-Vis absorption spectrum of $CsSnI_3$ thin film. Absorption cut off is indicated by the arrow to be 982 nm.

XRD was used to determine the crystal structure and the phase of the fabricated $CsSnI_3$ thin film to ensure the $CsSnI_3$ thin film having the photoactive phase. Figure 13 shows the XRD pattern of the $CsSnI_3$ thin film, which exhibits an orthorhombic perovskite black phase with space group *Pnma*. This result agrees with literature[7] as shown in Figure 14.

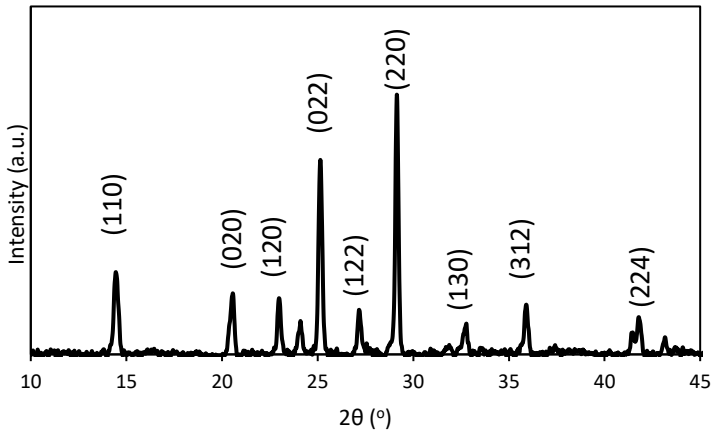

Figure 13. XRD pattern of the $CsSnI_3$ perovskite film on a glass substrate.

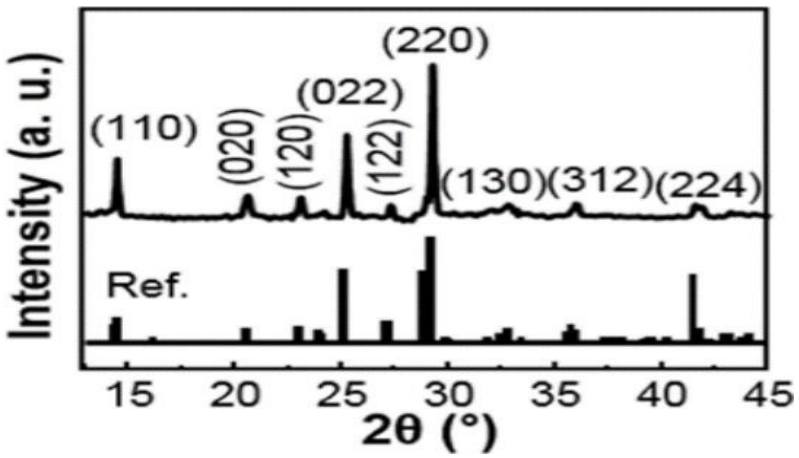

Figure 14. XRD pattern of the $CsSnI_3$ perovskite film on a glass substrate reported by Han et al. (2019).[7] Reference of the orthorhombic-structure $CsSnI_3$ from JCPDS card no. 04-014-1737.[7]

3.4 Device performance

NiOx and $CsSnI_3$ thin films were deployed as HTL and active layer in inverted perovskite solar cells with the structure of glass/ITO/NiO_x/$CsSnI_3$/$PC_{60}BM$/BCP/Ag. Figure 15 shows an energy diagram resembling the device structure and showing the valence band maxima and the conduction band minima for each material used. Figures 16a and b show the device performance when using annealed 2 and 6 wt% NiO_x thin film as HTL, respectively. Table 1 shows the average value of open-circuit voltage (V_{oc}), short-circuit current density (J_{sc}), fill factor (FF), and PCE as well as the maximum PCE for the two conditions. When comparing the two conditions, it can be seen that the device with 6 wt% NiO_x HTL has clearly a superior performance overall. From Table 1, when using NiO_x with 6 wt% concentration, V_{oc}, J_{sc}, FF, and PCE have increased substantially. This increase of the photovoltaics parameters is mainly due to the enhanced coverage of the NiO_x HTL prepared with 6 wt% NiO_x. As shown in Figure 6, the NiOx film prepared with 6 wt% NiO_x becomes more densely packed and the number of pinholes decreases. The best J-V curve of the

device with 6 wt% NiOx HTL shows a V_{oc} and J_{sc}, of 0.54 V, 2.65 mA cm^{-2} and FF, and PCE of 68.5, and 0.977%, respectively. However, as shown in Figure 17, the J-V curves exhibit an abnormal current density change between ~0.4-0.7 V, indicating instability of the device. The V_{oc} of the best device performance fits in the high end of what has been published in literature for pure tin perovskite.[12-13] Although the 6 wt% NiO_x based device shows a better device performance, it lacks consistency. Table 1 shows a relatively large standard deviation in the V_{oc} which indicates that the film on the device is not very uniform and indicates the possibility of the increase presence of pinholes in some areas in the device. In addition, the J_{sc} is very low even for all inorganic perovskite materials as in the literature, J_{sc} of some inorganic pure tin materials has reached as high as 25.71 mA cm^{-2}.[13] This low J_{sc} value could be a result of the thickness of the HTL layer, which reduces the charge transport, lowering the J_{sc}.

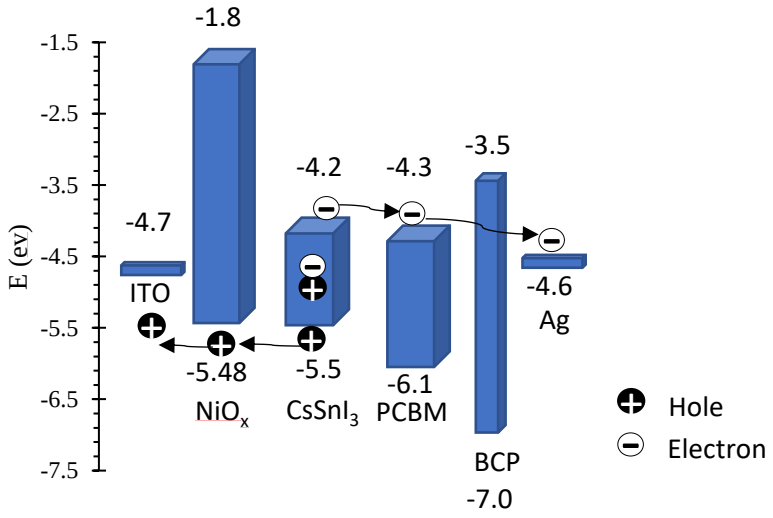

Figure 15. Energy diagram of the device structure showing the work function of two electrodes, and valence band maxima and the conduction band minima for HTL, ETL and active layer.

Table 1: Device performance of the devices with the HTL prepared by annealed 2 and 6 wt% NiO_x thin film.

HTL	V_{oc} (V)	J_{sc} (mA/cm^2)	FF (%)	PCE (%)	PCE_{max} (%)
2 wt% NiO_x	0.022±0.001	0.364±0.38	24.8±0.3	0.00177±0.002	0.0045
6 wt% NiO_x	0.37±0.16	3.24±0.70	47.5±18	0.56±0.35	0.997

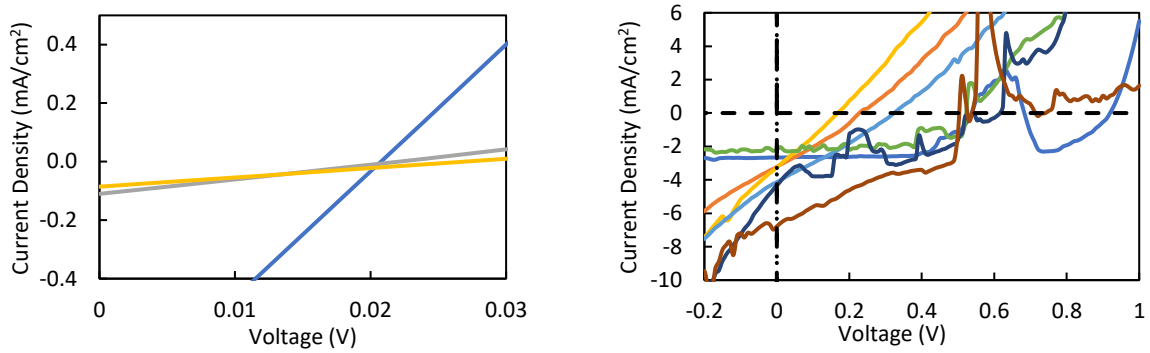

Figure 16. (a) J-V curves of the devices based on the 2 wt% NiO_x HTL. (b) J-V curves of the devices based on the 6 wt% NiO_x HTL. The curves are a resultant from different electrodes.

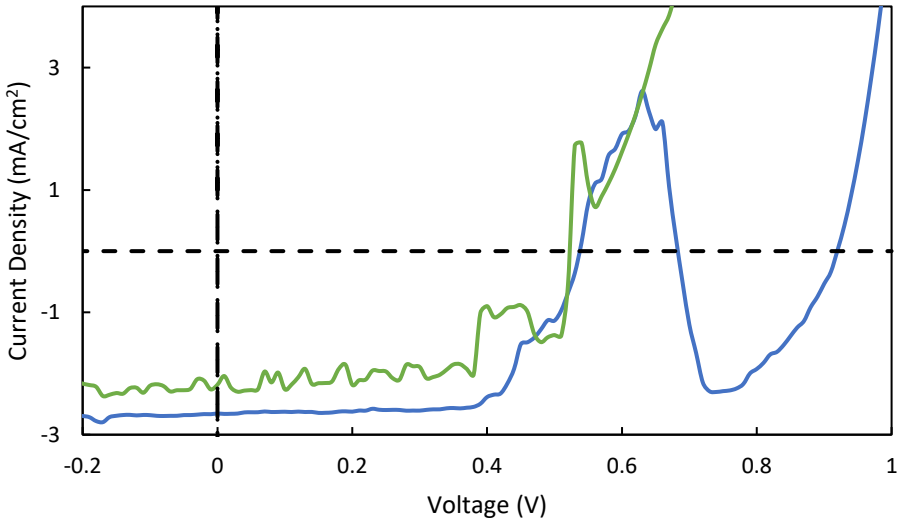

Figure 17. J-V curves of the best device performances based on the 6 wt% NiO_x HTL.

Chapter 4. Summery and Future Work

In this project, we synthesized NiOx NCs by a precipitation method, which was used as a hole transport layer in the $CsSnI_3$ perovskite solar cells. We explored the effect of annealing conditions, concentration of NiO_x ink and spin speed on the NiO_x film morphology and surface roughness. It was concluded that the concentration of the NiO_x ink affects the film morphology and surface roughness. As the concertation increases the film becomes more densely packed. In addition, the surface roughness increases as the concentration increases based on the average surface roughness value. In contrast, spin speed had no significant effect on surface roughness of NiO_x film. Annealing treatment of the NiO_x film resulted in more surface coverage and smaller, more uniform particles. Finally, we showed that the device performance improved when the concentration increased from 2 wt% to 6 wt% as a result of a better NiO_x film morphology.

We showed that NiO_x has a potential to substitute PEDOT:PSS for inorganic tin based perovskites based on the initial results obtained. NiO_x film thickness is a crucial parameter to consider as it affects the device performance directly. Optimizing NiO_x film thickness could help improve the device performance by enhancing the charge transport. Also, optimizing the annealing conditions will balance the nucleation and the growth rate enhancing the overall morphology of the NiO_x film. Thus, in the future work, film thickness and annealing condition optimization will be considered.

Wang et al. (2019) state that the $CsSnI_3$ film morphology has improved by adding antioxidant solvent additive triphenyl phosphite (TPPi) when making the precursor. When the film morphology was tested using SEM, it has been discovered that the films with higher concentration of TPPi has smaller size crystals with bigger interspaces, which indicates that

adding TPPi has enhanced the film morphology.[12] In addition, changing the molar ratio between CsI and SnI_2 could enhance the film morphology and ultimately enhancing the device performance. Song et al. explored different molar ratios between CsI and SnI_2 by fixing the SnI_2 concentration to 1 M and varying CsI concentration. They discovered that a molar ratio of 0.4:1 of CsI to SnI_2 enhanced the device performance.[13] Thus, In future making precursor, using different molar ratios of CsI and SnI_2 and using stabilizing additives such as TPPi will be considered and the effect on device performance will be studied.

Fullerene derivatives (PCBM) has been widely used as an electron transport layer (ETL) due to uniform and excellent electrical contact with the underlined perovskite and high electron mobility resulting in an excellent power conversion efficiency as high as 19.9%[9]. However, PCBM is very sensitive to water resulting the instability of the perovskite solar cell. Also, PCBM is considered very expensive, which hinders the large-scale industrial applications of the perovskite solar cells. Inorganic alternatives, such as Cadmium sulfide (CdS) and Cadmium selenide (CdSe) possess potential advantages in low material cost, charge mobility, moderate fabrication integration, and promising device stability.[9-10] Therefore, Cds and CdSe will be considered as a ETL substitute of PCBM.

References

[1]Green, M. A.; Ho-Baillie, A. Perovskite Solar Cells: The Birth of a New Era in Photovoltaics. *ACS Energy Letters* **2017**, *2* (4), 822–830.

[2]Zhang, Q., Hao, F., Li, J., Zhou, Y., Wei, Y., & Lin, H. (2018). Perovskite solar cells: must lead be replaced - and can it be done?. Science and technology of advanced materials, 19(1), 425–442. https://doi.org/10.1080/14686996.2018.1460176

[3]Wang, X.; Zhang, T.; Lou, Y.; Zhao, Y. All-Inorganic Lead-Free Perovskites for Optoelectronic Applications. *Materials Chemistry Frontiers* **2019**, *3* (3), 365–375.

[4]Chung I, Song JH, Im J, et al. CsSnI3: Semiconductor or metal? High electrical conductivity and strong near-infrared photoluminescence from a single material. High hole mobility and phase-transitions. *J Am Chem Soc*. 2012;134(20):8579-8587. doi:10.1021/ja301539s.

[5]Huang, L.-Y.; Lambrecht, W. R. L. Electronic Band Structure, Phonons, and Exciton Binding Energies of Halide Perovskites CsSnCl3, CsSnBr3, and CsSnI3. *Physical Review B* **2013**, *88* (16).

[6]Litzov, I.; Brabec, C. Development of Efficient and Stable Inverted Bulk Heterojunction (BHJ) Solar Cells Using Different Metal Oxide Interfaces. *Materials* **2013**, *6* (12), 5796–5820.

[7]Han, J. S.; Le, Q. V.; Choi, J.; Kim, H.; Kim, S. G.; Hong, K.; Moon, C. W.; Kim, T. L.; Kim, S. Y.; Jang, H. W. Lead-Free All-Inorganic Cesium Tin Iodide Perovskite for Filamentary and Interface-Type Resistive Switching toward Environment-Friendly and Temperature-Tolerant Nonvolatile Memories. *ACS Applied Materials & Interfaces* **2019**, *11* (8), 8155–8163.

[8]Weber, S.; Rath, T.; Mangalam, J.; Kunert, B.; Coclite, A. M.; Bauch, M.; Dimopoulos, T.; Trimmel, G. Investigation of NiOx-Hole Transport Layers in Triple Cation Perovskite Solar Cells. *Journal of Materials Science: Materials in Electronics* **2017**, *29* (3), 1847–1855.

[9]Jia, J.; Wu, J.; Dong, J.; Fan, L.; Huang, M.; Lin, J.; Lan, Z. Cadmium Sulfide as an Efficient Electron Transport Material for Inverted Planar Perovskite Solar Cells. *Chemical Communications* **2018**, *54* (25), 3170–3173.

[10]Tan, F., Xu, W., Hu, X. *et al.* Highly Efficient Inverted Perovskite Solar Cells with CdSe QDs/LiF Electron Transporting Layer. *Nanoscale Res Lett* **12,** 614 (2017).

[11]Marshall, K. P.; Walton, R. I.; Hatton, R. A. Tin Perovskite/Fullerene Planar Layer Photovoltaics: Improving the Efficiency and Stability of Lead-Free Devices. *Journal of Materials Chemistry A* **2015**, *3* (21), 11631–11640.

[12]Wang, Y.; Tu, J.; Li, T.; Tao, C.; Deng, X.; Li, Z. Convenient Preparation of CsSnI3 Quantum Dots, Excellent Stability, and the Highest Performance of Lead-Free Inorganic Perovskite Solar Cells So Far. J. Mater. Chem. A 2019, 7, 7683.

[13]Song, T.-B.; Yokoyama, T.; Aramaki, S.; Kanatzidis, M. Performance Enhancement of Lead-Free Tin-Based Perovskite Solar Cells with Reducing Atmosphere-Assisted Dispersible Additive. **2019**.